Hydrodynamic Transport of Excitons in Semiconductors and Bose-Einstein Condensation

Bennett Link[1] and Gordon Baym[1],[2]

[1]*Los Alamos National Laboratory, Los Alamos, New Mexico 87545*

[2]*Loomis Laboratory of Physics, University of Illinois, Urbana, Illinois 61801*

(Received 4 August 1992)

We study the expansion of an exciton gas against lattice drag, describe the transition between the diffusive and low-drag hydrodynamic regimes, and compare with experimental data obtained at exciton densities and temperatures near the Bose-Einstein phase boundary. As we show through numerical simulation, the rapid expansion of the exciton cloud seen experimentally at high exciton densities can be explained as drag-free hydrodynamic flow. Such a reduction in drag strongly suggests that Bose-Einstein condensation has occurred and that excitonic superfluidity is being observed.

PACS numbers: 71.35.+z, 64.60.−i

A dense gas of excitons (electron-hole bound states), produced by laser photoexcitation of a semiconductor at low temperature, is an ideal system with which to study the physical properties of a Bose-Einstein quantum gas [1]. Several properties of exciton systems make them suited for direct observation of Bose-Einstein condensation: (1) The exciton gas density, determined by the laser power, can be controlled; (2) the low exciton mass allows condensation at low densities; and (3) recombination luminescence in many cases reflects the energy distribution of the gas. Degenerate Bose-Einstein statistics have been reported for excitons in Ge [2] and biexcitons in CuCl [3]; however, a clear demonstration of Bose-Einstein condensation has yet to appear. In a recent study by Snoke, Wolfe, and Mysyrowicz of time- and space-resolved luminescence of orthoexcitons in Cu_2O, information was obtained on the kinetics of the thermodynamic quantities at the onset of condensation [4]. For a large range in temperature and density, the system appeared to be in the region of the condensation phase boundary (variation of density with temperature as $n \propto T^{3/2}$). This behavior likely represents the first experimental signature of quantum saturation, central to Bose condensation.

In a subsequent experiment, recombination luminescence of both orthoexcitons and the lower-lying paraexcitons in Cu_2O was studied ([5] hereafter SWM). At high excitation levels, the paraexciton density exceeds the critical density for condensation, and the energy spectrum develops a structure that cannot be described in terms of a thermalized Bose-Einstein distribution. Moreover, rapid expansion of the orthoexciton gas is observed at the highest densities, in contrast to the diffusive behavior seen at lower densities. SWM interpret the change in the exciton energy distribution and the rapid expansion of the orthoexciton gas as evidence for Bose-Einstein condensation and superfluid transport.

In this Letter we study the hydrodynamic expansion of an exciton gas against the drag force of the lattice. We describe the transition between the high-drag diffusive and low-drag hydrodynamic regimes. Comparison of our results with the measurements of SWM strongly suggests that the "ballistic" character of the expansion seen at high densities is indeed due to a marked reduction of the drag, implying that condensation has occurred and that superfluidity is being observed.

In the experiment of SWM, high-purity Cu_2O crystals immersed in superfluid helium are excited by a cavity-dumped Ar^+ laser. The laser is focused on a spot ~ 100 μm in diameter, producing a dense plasma of electrons and holes to a depth of the laser absorption length, ~ 1.6 μm. The absorbed power is up to 10^7 W cm^{-2} during an 8-ns pulse. The pairs thermalize by the emission of optical photons and combine into excitons in less than ~ 1 ns [6], and expand into the lattice at velocities comparable to the sound speed ($\sim 10^5$–10^6 cm s^{-1}). Excitons in Cu_2O have a binding energy $\simeq 0.15$ eV and a Bohr radius $\simeq 7$ Å [7]. Because of the relatively short laser absorption length, the excitons are effectively inertially confined, and the exciton density in the initial "pancake" can exceed 10^{19} cm^{-3}. Orthoexcitons decay in nanoseconds by radiative recombination or conversion into paraexcitons, which have lifetimes of microseconds [8]. (Paraexcitons lie lower than the orthoexcitons by an electron-hole exchange energy of 12 meV, and have much weaker luminescence than the orthoexcitons.) The densities of both species vary considerably with time as the gas undergoes expansion and recombination. Collision times for excitons are picoseconds [5], so that the ortho and paraexcitons remain in thermal equilibrium at a common temperature. However, because the conversion time between ortho and paraexcitons is considerably longer than the collision time, chemical equilibrium is not maintained, and the ortho and paraexcitons can have different chemical potentials.

The primary source of drag as the exciton gas expands into the lattice is the scattering of excitons with acoustic phonons. The interaction times are of order nanoseconds [5], comparable to the sound crossing time of the expanding exciton cloud, suggesting that the exciton transport is primarily diffusive. However, if an exciton gas is created with a density exceeding the critical density for Bose-Einstein condensation, the gas forms a bosonic superfluid, and the condensate moves relative to the lattice without

dissipation [9]. In this case the exciton gas penetrates farther into the crystal than if the motion were diffusion limited. We now study, through the use of an idealized one-component model, how such a reduction of drag would manifest itself in the dynamics of the exciton gas.

The dynamics of a collision-dominated fluid are governed by the equations of hydrodynamics, which in the absence of viscosity read

$$\frac{\partial \rho}{\partial t}+\nabla\cdot\rho\mathbf{v}=0\,, \tag{1}$$

$$\left[\frac{\partial}{\partial t}+\mathbf{v}\cdot\nabla\right]\mathbf{v}=-\frac{\nabla p}{\rho}-\frac{\mathbf{v}}{\tau}\,, \tag{2}$$

where ρ is the mass density of the gas, p is its pressure, and τ is the time scale for momentum loss from the gas (to phonons in this case). For adiabatic motion $dp=c^2d\rho$, where c is the adiabatic sound speed. We consider flows near the sound velocity over a length scale L, so that $\nabla p\sim c^2\rho/L$. The viscous force $\eta\nabla^2 v$ is $\sim\eta c/L^2\sim\rho\tau_s c^3/L^2$, where η is the viscosity and τ_s is the scattering time in the gas. Hence $\eta|\nabla^2 v/\nabla p|\sim\tau_s c/L$ which is $\ll 1$ for $\tau_s\sim 1$ ps, $c\sim 10^6$ cm s^{-1}, and $L\sim 10$ μm, and the neglect of viscosity is justified. Equations (1) and (2) are useful for studying the transition between diffusive and drag-free behavior as τ is varied. The character of the two limits can be seen by considering small perturbations δp and $\delta\rho$ in the pressure and density. We obtain the linear equation

$$\frac{\partial^2\delta\rho}{\partial t^2}-c^2\nabla^2\delta\rho+\frac{1}{\tau}\frac{\partial\delta\rho}{\partial t}=0\,, \tag{3}$$

which yields the dispersion relation, $\omega^2+i\omega/\tau-c^2k^2=0$ for perturbations of wave number k. In the limit $ck\tau\gg 1$, we have $\omega^2\simeq c^2k^2$, corresponding to ordinary sound propagation. In this limit the cloud in general undergoes drag-free (Riemann) expansion. In the limit $ck\tau\ll 1$, the system has the usual diffusive mode with frequency $\omega=-i(c^2\tau)k^2$, and a damped mode of frequency $-i/\tau$. The values of c, k, and τ change over the evolution of an exciton cloud; to set the scale, note that for a cloud of size 10 μm, a sound speed $c\sim 10^6$ cm s^{-1}, and $\tau\sim 1$ ns, one has $ck\tau\sim 1$.

We now turn to numerical solutions of the nonlinear equations (1) and (2). In this initial investigation we neglect entropy production due to drag against the lattice, the effects of recombination in the gas and at the crystal surface, and conversion reactions between ortho and paraexcitons, effects which eventually must be taken into account. For adiabatic flow we must specify an equation of state at fixed entropy per particle σ. We expect the interaction corrections to the equation of state to be small since for an exciton density as high as $n=10^{20}$ cm^{-3}, and an exciton Bohr radius $a=7$ Å, one has $na^3\ll 1$. We therefore take the equation of state for the exciton gas (ortho plus para) to be that of a weakly interacting gas, $p\propto\rho^{5/3}$ at fixed σ, which implies $c\propto\rho^{1/3}$ (we note that in a very-low-temperature weakly interacting Bose-Einstein gas, the sound speed varies as $\rho^{1/2}$, so that taking $c\propto\rho^{1/3}$ is qualitatively correct even in this regime). Most of the exciton mass flows directly into the crystal, so we consider one-dimensional planar expansion ($x\geq 0$).

During a laser pulse, typically 10 ns in duration, the exciton number density varies significantly as exciton creation competes with recombination and expansion. After their creation by the pulse, the thermal energy of the excitons drives acceleration into the crystal. The excitons deepest in the crystal move the fastest, as they have undergone the most acceleration, while the excitons near the crystal surface will be nearly at rest. The exact density and velocity distributions immediately following the laser pulse are determined by the creation rate of excitons at and near the crystal boundary during the laser pulse, the local recombination rate (a function of density), and the effectiveness of radiative (and phonon wind) energy transport into the crystal. Our goal is to study the late-time behavior, which is in fact relatively insensitive to the choice of initial velocity and density profiles. Thus, at this stage we do not attempt to model the time-dependent creation process; instead, we choose as a reasonable initial condition immediately following the laser pulse a Gaussian distribution in density, with its maximum at the crystal boundary ($x=0$). We assume no appreciable exciton flux at the crystal boundary, so that $v=0$ at $x=0$, and take an initial velocity distribution, $v(x)=\alpha[c_0-c(x)]$ for $x\geq 0$, where $c(x)$ is the initial sound speed, a function of x through the dependence of ρ on position, c_0 is the initial sound speed at $x=0$, and α is a constant. We present results for the arbitrary value $\alpha=2$, but find that the results depend only weakly on this choice.

The expansion is characterized by two length scales: $c_0\tau$, and the width of the initial distribution. More precisely, we define the half-width Δ, following SWM, as the distance from the crystal surface to the point in the gas distribution at which the density is half that at the surface; Δ_0 is the initial value of Δ. At late times, when the expanding cloud is large compared to its initial size, the solutions take the form $\rho/\rho_0=f(x/c_0\tau,t/\tau)$ and $v/c_0=g(x/c_0\tau,t/\tau)$. In Riemann expansion ($\tau=\infty$) at late times, ρ and v are functions of x/t only, and the expansion is scale-free. In Fig. 1 we show numerical solutions to (1) and (2) for Δ, in units of Δ_0, as a function of time, in units of Δ_0/c_0, for different values of τ. For small drag (large τ), the system undergoes Riemann expansion at a velocity comparable to c_0. For large drag (small τ), however, the expansion is diffusive, with $\Delta\propto t^{1/2}$.

SWM have determined the width of the expanding exciton gas formed by laser pulses of variable power by measuring the orthoexciton recombination luminescence; we show these data in Fig. 2. The laser pulse begins at $t=0$, and deposits most of its energy by 12 ns. At the lowest power (bottom curve), the expansion is diffusive. At the highest laser power (top curve), corresponding to

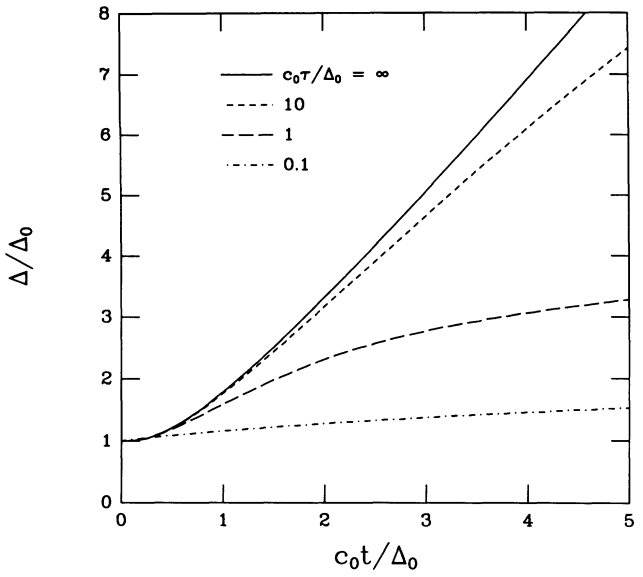

FIG. 1. The half-width of the expanding distribution vs c_0t for different values of the drag.

the highest exciton density, the expansion assumes a "free" character which SWM interpret as nearly dissipationless motion of a condensate. We model the data by solving the full hydrodynamics for times $t \geq 12$ ns, fitting c_0 and τ by eye with particular attention to reproducing the late-time behavior (when the choices of the initial velocity and density distributions become unimportant); our results are shown in Fig. 2. The fitted values of c_0 and τ increase with laser power. Indeed, at the highest power, the gas appears to expand without drag against the lattice. At the lowest laser power, SWM obtain a diffusion coefficient $D \simeq 700$ cm^{2}s^{-1} from the measured widths. With the fitted values $c_0 = 3.1 \times 10^5$ cm s^{-1} and $\tau = 10$ ns, the diffusion coefficient in the linear analysis $D = c^2\tau$ equals 960 cm^{2}s^{-1}, close to the estimate of SWM; the difference arises from the decrease of c with time.

In Fig. 3 we show the density and velocity profiles of the gas at different times as a function of position in the crystal. The greater penetration of the cloud into the crystal is evident for lower drag [see Fig. 3(a)]. At late times the velocity profile scales as $v = x/t$ for $x \lesssim 100$ μm. The velocity, while remaining monotonic with x at low drag, develops a crested structure at late times for the case of high drag [Fig. 3(c)]. The crest develops as the gas near the crystal boundary is driven by its pressure into the decelerating gas deeper in the crystal. One expects the expansion rate to increase with laser power, since the initial gas density and pressure become higher. However, the data are not well fit by an increase in density alone; in Fig. 4 we show the results of varying c_0 only, with τ held fixed at 10 ns, the value that fits the lowest-power data.

In summary, our numerical simulations support the conclusion of SWM that the rapid expansion of the exciton gas observed at the highest laser powers indicates a

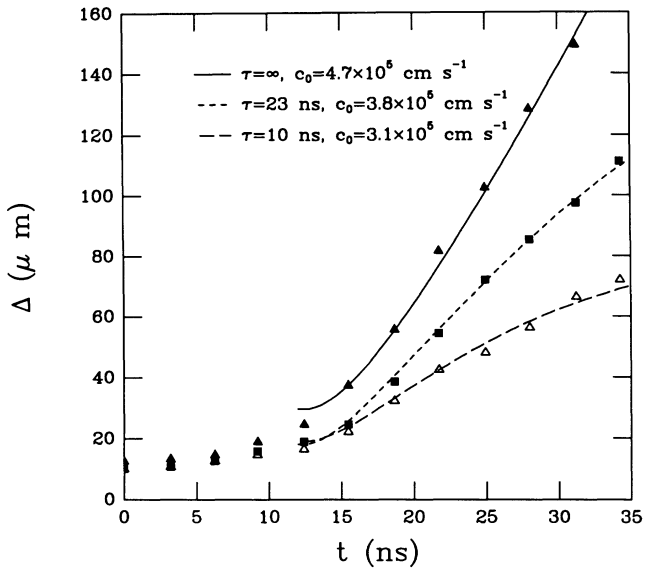

FIG. 2. The half-width as a function of time for three different laser powers; the data are from SWM. The laser pulse is about 10 μs in duration, and begins at $t = 0$. Solid triangles correspond to a laser power of 5×10^{-5} μJμm^{-2}, solid squares to 1.5×10^{-5} μJμm^{-2}, and open triangles to 10^{-8} μJμm^{-2}. The curves are numerical solutions using the values of τ and c_0 indicated.

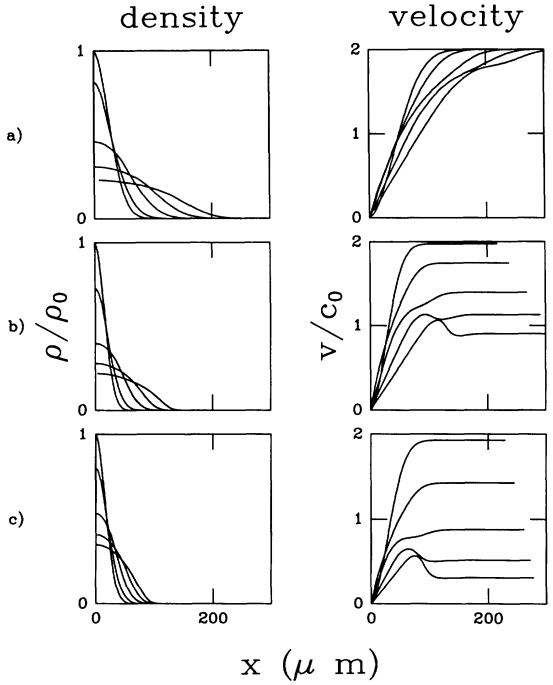

FIG. 3. Density and velocity profiles for the numerical solutions of Fig. 2, at times $t = 12$, 15, 20, 25, and 30 ns for (a) $\tau = \infty$, (b) $\tau = 23$ ns, and (c) $\tau = 10$ ns.

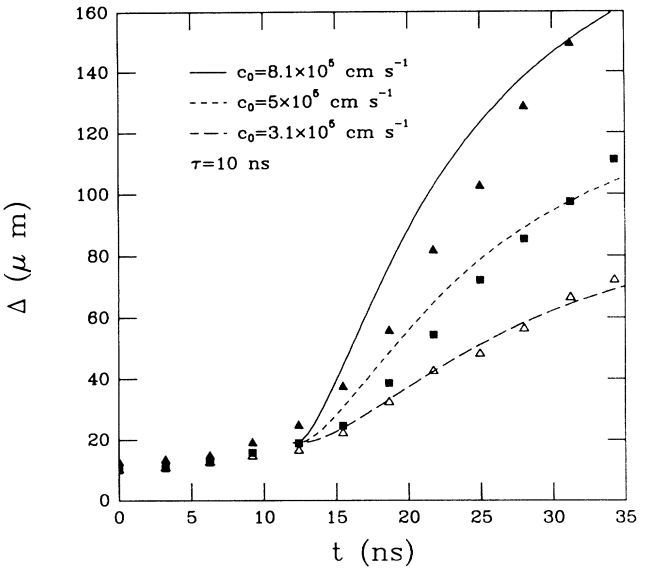

FIG. 4. Same as Fig. 2, but with constant $\tau = 10$ ns and variable c_0 in the numerical solutions.

substantial reduction of drag. This observation, coupled with the structure seen in the paraexciton energy distribution, provides compelling evidence for the onset of excitonic Bose-Einstein condensation and superfluidity. A complete description will require using an improved equation of state and taking into account the differences in the dynamics of the normal and superfluid components. One must also account for the finite exciton lifetime, i.e., recombination throughout the gas and at the crystal surface, entropy production associated with the lattice drag, and finite-temperature effects of the lattice. An alternative mechanism for the rapid transport of an exciton cloud, involving acceleration by a phonon wind, has been discussed by Bulatov and Tikhodeev [10]; such effects must also be considered in a complete description of the expansion process. Open problems also include a theoretical determination of the density dependence of the drag time τ.

We are grateful to J. Wolfe and D. Snoke for many valuable discussions of this problem, and for a critical reading of the manuscript. This work was supported in part by National Science Foundation Grants No. DMR 88-18713 and No. DMR 91-22385.

[1] E. Hanamura and H. Haug, Phys. Rep. **33**, 209 (1977); A. Mysyrowicz, J. Phys. (Paris) **41**, Suppl. 7, 281 (1980); C. Comte and P. Nosières, J. Phys. (Paris) **43**, 1069 (1982); **44**, 1083 (1982).

[2] V. B. Timofeev *et al.*, in *Proceedings of the Sixteenth International Conference on Physics of Semiconductors, Montpellier, France, 1982,* edited by M. Averous (North-Holland, Amsterdam, 1983), p. 327.

[3] N. Peghambarian, L. L. Chase, and A. Mysyrowicz, Phys. Rev. B **27**, 2325 (1983).

[4] D. Snoke, J. P. Wolfe, and A. Mysyrowicz, Phys. Rev. Lett. **59**, 827 (1987).

[5] D. Snoke, J. P. Wolfe, and A. Mysyrowicz, Phys. Rev. B **41**, 11171 (1990).

[6] N. Caswell, J. S. Weiner, and P. Y. Yu, Solid State Commun. **40**, 843 (1981).

[7] For a review of the properties of Cu_2O, see V. T. Agekyan, Phys. Status Solidi A **43**, 11 (1977).

[8] D. P. Trauernicht, J. P. Wolfe, and A. Mysyrowicz, Phys. Rev. Lett. **52**, 855 (1984); D. P. Trauernicht, J. P. Wolfe, and A. Mysyrowicz, Phys. Rev. B **34**, 2561 (1986).

[9] V. A. Gergel, R. F. Kazarinov, and R. A. Suris, Zh. Eksp. Teor. Fiz. **54**, 298 (1968) [Sov. Phys. JETP **27**, 159 (1968)].

[10] A. Bulatov and S. Tikhodeev (to be published).